2011 11th IEEE International Conference on Nanotechnology
Portland Marriott
August 15-18, 2011, Portland, Oregon, USA

A Spectrally-Tunable Photocurrent Microscope for Characterizing Nanoelectronic Devices

Tristan DeBorde, Joshua W. Kevek, Tal Sharf, Jenna L. Wardini, Ethan D. Minot
Department of Physics, Oregon State University, Corvallis, OR, 97331-6507
Email: minote@physics.oregonstate.edu

***Abstract* — Scanning photocurrent microscopy is a unique tool that facilitates both device characterization and the study of fundamental properties of optoelectronic nanomaterials. We have built a scanning photocurrent microscope that incorporates a super continuum laser as the light source. The microscope illuminates nanoelectronic devices with a micron-scale light spot and a photon energy that is tunable from 0.67 eV to 2.7 eV. We describe the design of our microscope and present measurements of carbon nanotube transistor devices. These measurements highlight the features of our microscope, particularly the advantages of combining spatial and spectral resolution when characterizing nanoelectronic devices.**

Index Terms – Photocurrent, carbon nanotube, field-effect transistor

I. Introduction

Nanoscale materials often have unique and beneficial electronic and optoelectronic properties [1]. For example, recent studies of carbon-based optoelectronic devices have shown promise in the fields of photodetection, high-speed optical communications, and solar energy conversion [2-4].

Scanning photocurrent microscopy (SPCM), and the closely related technique of scanning photoconductivity microscopy, are versatile methods for investigating optoelectronic properties of nanoelectronic devices [4-6]. In both techniques, a focused laser spot is raster scanned across a device while recording current (see Fig. 1). Fig. 1b shows an SPCM image superimposed on top of an atomic force microscopy (AFM) height image of a carbon nanotube field effect transistor (CNT FET). The color of each pixel corresponds to the measured current when the laser spot is centered on the x-y coordinates of the pixel. This measurement technique has been used with single-wavelength laser sources to investigate the optoelectronic properties of nanomaterial-metal interfaces (nanowire-metal, CNT-metal, and graphene-metal) [7-11] and nanoelectronic devices with other sources of built-in electric fields [4, 12].

Additional information about nanoelectronic devices can be gained by using a wavelength-tunable light source. Freitag et al. used wide-field illumination with a tunable Ti-Sapphire laser to measure resonant photoconductivity in CNT FETs [13]. Lee et al. used wide-field wavelength-tunable illumination from a monochromated white light source to investigate photocurrent resonances in CNT *p-n* junctions [12]. More recently, a tunable light source was combined with a scanning microscope to give both spatial and spectral resolution [4]. Gabor et al. used this technique

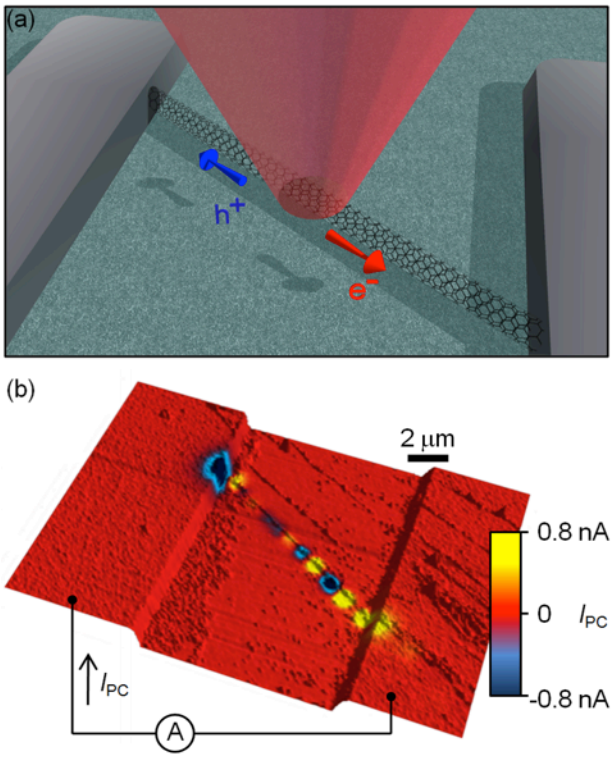

Fig. 1 SPCM Measurement Example. (a) Cartoon diagram of a scanning photocurrent measurement. (b) SPCM image from a CNT FET device taken at 632 nm, 800 μW, and FWHM of approximately one micron. The photocurrent image has been superimposed onto an AFM height image of the device. The other nanotubes in the image do not make it across the electrode gap and show no photocurrent response.

to measure multiple electron generation in CNT photodiodes [4].

The goal of our current work is to expand the capabilities of spectrally-tunable SPCM. Here we describe the construction of an SPCM instrument with a light source that has an extremely tunable spectral range and sample intensities above 5 kW/cm^2 per nanometer of bandwidth.

II. Microscope Design

Our SPCM instrument diagramed in Fig. 2, uses a Fianium super continuum laser (SC-450) as the primary light source. The super continuum outputs a wide wavelength range between 450 nm – 1800 nm with a roughly constant spectral power density (4 W total output power). A monochromator (Micro HR, *Horiba*) is used to select and control the output wavelength and bandwidth. The typical

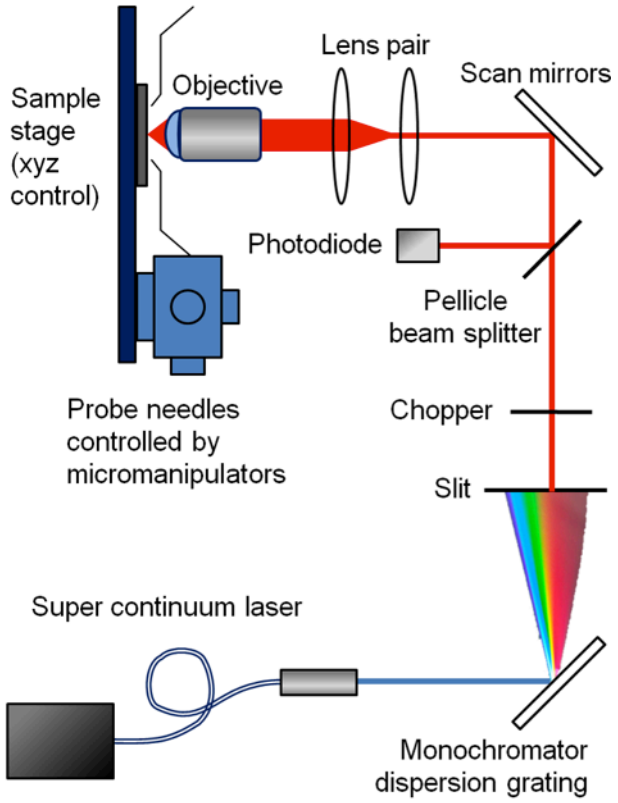

Fig. 2 Schematic Diagram of Scanning Photocurrent Microscope.

output bandwidth used for the measurements reported here was approximately 5 nm. In this configuration we are able to deliver a few hundred micro-watts of power to the sample with a micron scale spot size in the visible spectrum.

We use a pair of scan mirrors (OHF-7, QD-4000, *Nutfield Technology*) to control the laser position on the sample. A pair of lenses (Achromatic Doublets with focal lengths of 5.0 cm and 7.5 cm, *Thorlabs*) is placed between the scan mirrors and the objective. This pair of lenses ensures that the collimated light source is centered in the middle of the back plane of the objective for all scan mirror angles.

For some applications it is desirable to increase excitation bandwidth to increase excitation power. However, opening the exit slit of the monochromator to increase bandwidth adversely affects image resolution due to the dispersion from the monochromator grating. A planned improvement to our setup is the use of a double monochromator operated in subtractive mode to remove the dispersion from the monochromated beam.

An additional feature that we have incorporated in our instrument is reflection imaging. Reflection images can be acquired simultaneously with photocurrent images, allowing us to determine laser position relative to the metal electrode structure. A pellicle beam splitter (92:8, *Thorlabs*) directs reflected light to a photodiode (PDA100A, *Thorlabs*). The electrodes (patterned thin metal films) reflect more strongly than the SiO_2/Si substrate.

Reflection imaging is also a convenient method of determining laser spot size (Fig. 3). We define the normalized reflection R_N as

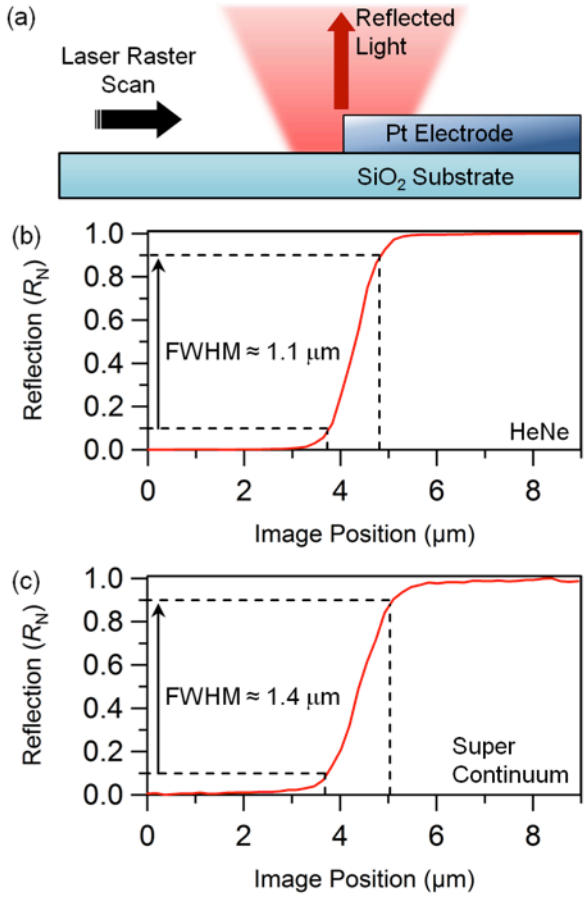

Fig. 3 Spot Size Characterization from Reflection Images. (a) Cartoon diagram of laser spot halfway onto a metal electrode corresponding to $R_N = 0.5$. (b) R_N of electrode edge from HeNe laser. (c) R_N of electrode edge from super continuum laser with monochromator output set to 632.8 nm and 1 nm bandwidth.

$$R_N = \frac{R - R_{Si}}{R_M - R_{Si}}, \quad (1)$$

where R is the measured reflection signal, R_{Si} is the reflection from the SiO_2/Si substrate and R_M is the reflection from the metal electrode. Fig. 3b shows R_N as a HeNe laser is scanned across the abrupt edge of a metalized area. The full-width at half max (FWHM) is estimated to be 1.1 μm. A similar FWHM is found for the super continuum light source when the bandwidth output is set to one nanometer. The focusing objective is a 50x, extra long working distance objective with a numerical aperture of 0.55 (CFI LU Plan BD ELWD 50X A, *Nikon*).

III. Results and Discussion

A. *Photocurrent Imaging of a Typical CNT FET Device*

An AFM height image and transistor curve for an ambipolar CNT FET device is shown in Fig. 4. The device is made using chemical vapor deposition (CVD) growth of CNTs and standard photolithography techniques as described in [14]. The transistor curve in Fig. 4b shows a large amount of advancing hysteresis when sweeping the gate voltage (V_g). Fig. 4b shows that when V_g = 0 V the device is p-type (Fermi energy below the band gap) and when V_g = 10 V the device is n-type (Fermi level above the band gap) if dV_g/dt is sufficiently fast.

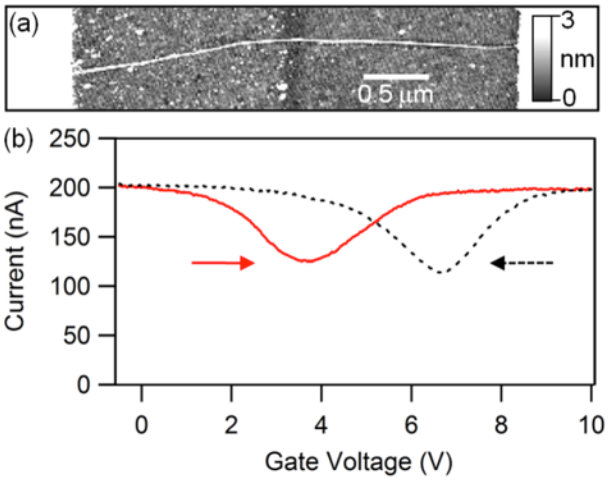

Fig. 4 Ambipolar CNT FET (a) AFM Height image of CNT on SiO_2 crossing electrode gap. Scale bar is 0.5 µm. (b) Transistor curve of device. The solid (dashed) curve is an increasing (decreasing) V_g sweep. V_{sd} = 25 mV, dV_g/dt = 0.5 V/s.

To study the optoelectronic properties of this device we performed SPCM imaging at different gate voltages. Fig. 5a shows a photocurrent image obtained at V_g = 0 V and with no bias across the source and drain electrodes (V_{sd} = 0 V, same configuration as Fig. 1b). There are clear photocurrent spots visible at the left and right CNT-metal interfaces. A similar image was taken immediately after sweeping V_g to +10 V (Fig. 1c). With the Fermi level in the conduction band, the polarity of the photocurrent spots switches sign.

Photocurrents generated at CNT-electrode interfaces have been studied by several previous authors [5, 8, 9, 15]. The effect is typically attributed to a photoelectric effect, whereby the built-in electric field at a CNT-metal interface drives the photo-excited carriers either toward or away from the metal [8, 9]. Thus, the polarity of this interfacial photocurrent is thought to depend on whether the CNT FET is operating in a p-type or n-type regime.

The reversal of photocurrent polarity observed in Fig. 5c is not permanent and appears related to the device hysteresis. Photocurrent measurements were acquired for several minutes after V_g was swept from 0 V to 10 V and then held at 10 V (Fig. 5d-h). Each image took 30 seconds to acquire. As time progresses we can visualize the hysteresis advance as it affects the photocurrent response. By the last image, V_g = 10 V, t = 410 s, the photocurrent closely resembles the starting structure shown in Fig. 5a where V_g = 0 V.

Previous work by Lee et al. proposed that charge transfer between the CNT and silanol charge traps residing at the SiO_2-air interface causes advancing hysteresis in unpassivated CNT FET devices [16]. We conjecture that the photocurrent evolution shown in Fig. 5 reflects this migration of charge on the device surface, which eventually nullifies the applied gate voltage.

Hysteresis presents a challenge for many potential studies of optoelectronic properties. The Fermi energy of the CNT cannot be held at a stable level to allow detailed studies. One approach to solve this problem is passivation by dielectric encapsulation [17]. A second strategy to reduce

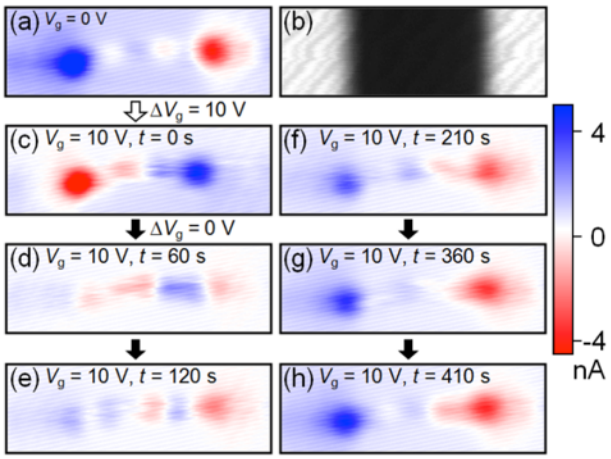

Fig. 5 Imaging CNT FET Hysteresis (a) SPCM image of device in Fig. 4 at V_g = 0V (b) Corresponding reflection image of device. (c) SPCM image taken immediately after sweeping V_g to 10 V. (d)-(h) Multiple SPCM images showing transient photocurrent behavior while V_g is held at 10 V. (d) t = 60 seconds (e) t = 120 seconds (f) t = 210 seconds (g) t = 360 seconds (h) t = 410 seconds.

hysteresis, described below, is to use suspended CNT FET devices.

B. Photoconductivity Spectrum of a Suspended CNT FET

Fig. 6a shows the transistor behavior of a suspended semiconducting CNT. As seen by previous authors [18], the suspended device geometry shows significantly less hysteresis than surface-bound CNT FETs. The CNT bridges a pair of Pt electrodes that are separated by a 1 µm gap that is 1 µm deep (see inset to Fig. 6a). Details of the fabrication steps will be reported by Sharf et al. [19]. A reflection image and short-circuit photocurrent image of the device are shown in Fig. 6b and c respectively. The reflection image clearly shows the Pt electrodes and the islands of catalyst that were

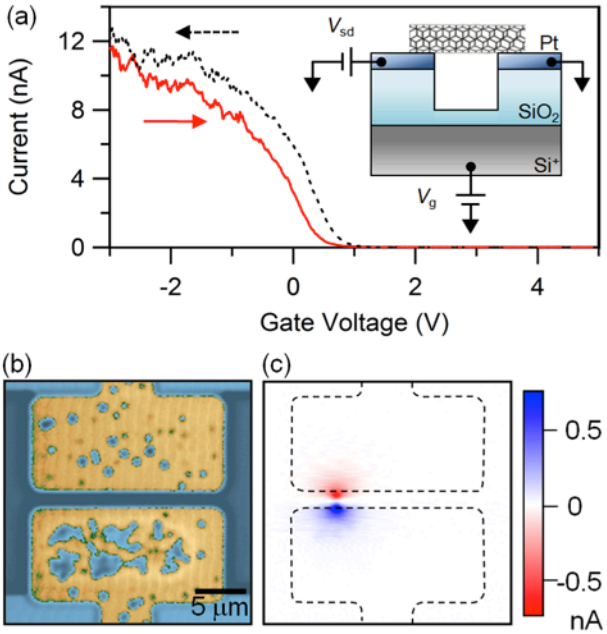

Fig. 6 Suspended CNT FET with Large Band Gap (a) Transistor curve of device. V_{sd} = 25 mV, dV_g/dt = 0.5 V/s. Inset shows device geometry (b) Reflection image of device. (c) Short circuit photocurrent image of device taken with lock-in amplifier.

placed on top of the Pt to facilitate growth of CNTs by chemical vapor deposition.

Fig. 7 shows the spectrally-resolved photoconductivity of the suspended CNT. The monochromated light source was focused on the center of the suspended CNT (half-way between the photocurrent spots seen in Fig. 6c). The gate voltage was set to 1.8 V, ensuring that the transistor was in the off state (depleted of charge carriers). A dc bias of 200 mV was applied between the source and drain electrodes. The monochromated light source was chopped at 3 kHz and was varied from 455 nm (2.73 eV) to 750 nm (1.65 eV). The photoinduced current was measured with a lock-in amplifier (SR830, *SRS*). The spectral response shows sharp resonances at 1.82 eV and 2.17 eV. The spectral power density of the light source is shown in Fig. 7b. Clearly, the spectral peaks in the photoinduced current are not related to the incident power of the light source.

Resonant photoconductivity of a semiconducting CNT was previously measured by Freitag et al. The authors observed peaks in the range 1.3-1.45 eV which they assigned to the E_{22} transition since the average diameter of these nanotubes was approximately 1.3 nm [13]. Similarly, we tentatively assign the resonances measured in our device to the E_{33} and E_{44} transitions in a CNT of diameter approximately 2.0 nm. The less intense, broad feature 200 meV above the 2.17 eV peak is likely related to a phonon-coupled transition [20].

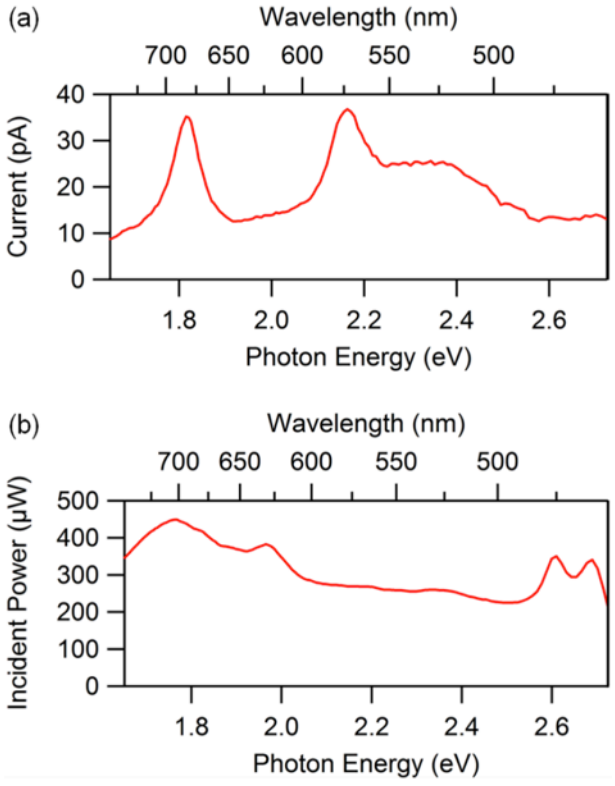

Fig. 7 Spectral Dependence of Suspended CNT FET. (a) Measured change in current as photon energy is varied. (b) Power incident to sample as a function of photon energy.

V. Summary and Conclusion

We have described our newly constructed a SPCM instrument that is capable of micron resolution imaging across a wide spectral range. Preliminary results demonstrate both spatial and spectral characterization of nanoscale optoelectronic devices. SPCM imaging on surface bound CNTs illustrates the challenges associated with hysteretic effects. A photoconductivity measurement of a suspended CNT FET shows resonances near 1.82 eV and 2.17 eV. Promising directions for future research include chirality assignment of the CNTs in FET devices and studies of the wavelength dependent efficiency of photocurrent generation in CNT and graphene photodiode devices.

Acknowledgment

Acknowledgment is made to the Donors of the American Chemical Society Petroleum Research Fund for the support of this research. Additional support for this work was provided by the Oregon Nanoscience and Microtechnology Institute (ONAMI). Sample fabrication was performed at the Cornell node of the National Nanofabrication Infrastructure Network, which is supported by the National Science Foundation (Grant ECS-0335765). We thank Nathan Gabor, Xiaodong Xu, and Jiwoong Park for several useful discussions.

References

[1] P. Avouris, *et al.*, "Carbon-nanotube photonics and optoelectronics," *Nature Photonics,* vol. 2, pp. 341-350, Jun 2008.

[2] F. N. Xia, *et al.*, "Ultrafast graphene photodetector," *Nature Nanotechnology,* vol. 4, pp. 839-843, Dec 2009.

[3] T. Mueller, *et al.*, "Graphene photodetectors for high-speed optical communications," *Nature Photonics,* vol. 4, pp. 297-301, May 2010.

[4] N. M. Gabor, *et al.*, "Extremely Efficient Multiple Electron-Hole Pair Generation in Carbon Nanotube Photodiodes," *Science,* vol. 325, pp. 1367-1371, Sep 11 2009.

[5] K. Balasubramanian, *et al.*, "Photoelectronic transport imaging of individual semiconducting carbon nanotubes," *Applied Physics Letters,* vol. 84, pp. 2400-2402, Mar 29 2004.

[6] M. Freitag, *et al.*, "Scanning photovoltage microscopy of potential modulations in carbon nanotubes," *Applied Physics Letters,* vol. 91, pp. -, Jul 16 2007.

[7] Y. Ahn, *et al.*, "Scanning photocurrent imaging and electronic band studies in silicon nanowire field effect transistors," *Nano Letters,* vol. 5, pp. 1367-1370, Jul 2005.

[8] M. Freitag, *et al.*, "Imaging of the schottky barriers and charge depletion in carbon nanotube transistors," *Nano Letters,* vol. 7, pp. 2037-2042, Jul 2007.

[9] Y. H. Ahn, *et al.*, "Photocurrent imaging of p-n junctions in ambipolar carbon nanotube transistors," *Nano Letters,* vol. 7, pp. 3320-3323, Nov 2007.

[10] F. N. Xia, *et al.*, "Photocurrent Imaging and Efficient Photon Detection in a Graphene Transistor," *Nano Letters,* vol. 9, pp. 1039-1044, Mar 2009.

[11] J. Park, *et al.*, "Imaging of Photocurrent Generation and Collection in Single-Layer Graphene," *Nano Letters,* vol. 9, pp. 1742-1746, May 2009.

[12] J. U. Lee, "Band-gap renormalization in carbon nanotubes: Origin of the ideal diode behavior in carbon nanotube p-n structures," *Physical Review B,* vol. 75, pp. -, Feb 2007.

[13] M. Freitag, *et al.*, "Photoconductivity of single carbon nanotubes," *Nano Letters,* vol. 3, pp. 1067-1071, Aug 2003.

[14] L. Prisbrey, *et al.*, "Controlling the Function of Carbon Nanotube Devices with Re-writable Charge Patterns," *Applied Physics Letters*, in submission.
[15] A. Mohite, *et al.*, "Field-enhanced photocurrent spectroscopy of excitonic states in single-wall carbon nanotubes," *Nano Letters,* vol. 6, pp. 1369-1373, Jul 12 2006.
[16] J. S. Lee, *et al.*, "Origin of gate hysteresis in carbon nanotube field-effect transistors," *Journal of Physical Chemistry C,* vol. 111, pp. 12504-12507, Aug 30 2007.
[17] W. Kim, *et al.*, "Hysteresis caused by water molecules in carbon nanotube field-effect transistors," *Nano Letters,* vol. 3, pp. 193-198, Feb 2003.
[18] M. Muoth, *et al.*, "Hysteresis-free operation of suspended carbon nanotube transistors," *Nature Nanotechnology,* vol. 5, pp. 589-592, Aug 2010.
[19] T. Sharf, *et al.*, "Fabriation of Low-Noise Carbon Nanotube Field-Effect Biosensors," in *Nanotechnology (IEEE-NANO), 2011 11th IEEE Conference on*, in submission.
[20] X. H. Qiu, *et al.*, "Photoconductivity spectra of single-carbon nanotubes: Implications on the nature of their excited states," *Nano Letters,* vol. 5, pp. 749-752, Apr 2005.